J Physiol 587.15 (2009) pp 3831–3849

The Journal of Physiology

Glycinergic input of widefield, displaced amacrine cells of the mouse retina

Sriparna Majumdar, Jan Weiss and Heinz Wässle

Department of Neuroanatomy, Max-Planck-Institute for Brain Research, Deutschordenstrasse 46, D-60528 Frankfurt/Main, Germany

Glycine receptors (GlyRs) of displaced amacrine cells of the mouse retina were analysed using whole cell recordings and immunocytochemical staining with subunit-specific antibodies. During the recordings the cells were filled with a fluorescent tracer and 11 different morphological types could be identified. The studies were performed in wild-type mice and in mutant mice deficient in the GlyRα1 (*Glra1*$^{spd-ot}$, 'oscillator' mouse), the GlyRα2 (*Glra2*$^{-/-}$) and the GlyRα3 subunit (*Glra3*$^{-/-}$). Based on their responses to the application of exogenous glycine in the retinas of wild-type and mutant mice, the cells were grouped into three major classes: group I cells (comprising the morphological types MA-S5, MA-S1, MA-S1/S5, A17, PA-S1, PA-S5 and WA-S1), group II cells (comprising the morphological types PA-S4, WA-S3 and WA-multi) and ON-starburst cells. For further analysis, spontaneous inhibitory postsynaptic currents (sIPSCs) were measured both in wild-type and mutant mouse retinas. Glycinergic sIPSCs and glycine induced currents of group I cells remained unaltered across wild-type and the three mutant mice (mean decay time constant of sIPSCs, $\tau \sim$25 ms). Group II cells showed glycinergic sIPSCs and glycine induced currents in wild-type, *Glra1*$^{spd-ot}$ and *Glra3*$^{-/-}$ mice ($\tau \sim$25 ms); however, glycinergic currents were absent in group II cells of *Glra2*$^{-/-}$ mice. Glycine induced currents and sIPSCs recorded from ON-starburst amacrine cells did not differ significantly between wild-type and the mutant mouse retinas ($\tau \sim$50–70 ms). We propose that GlyRs of group II cells are dominated by the α2 subunit; GlyRs of ON-starburst amacrine cells appear to be dominated by the α4 subunit.

(Received 18 February 2009; accepted after revision 15 June 2009; first published online 15 June 2009)

Corresponding author H. Wässle: Max-Planck-Institut für Hirnforschung, Deutschordenstr. 46, D-60528 Frankfurt/Main, Germany. Email: waessle@mpih-frankfurt.mpg.de

Abbreviations AII, AII amacrine cell; A17, A17 amacrine cell; DAD, drug application device; GCL, ganglion cell layer; *Glra2*$^{-/-}$, glycine receptor α2 knockout mouse; *Glra3*$^{-/-}$, glycine receptor α3 knockout mouse; *Glra1*$^{spd-ot}$, glycine receptor α1 deficient, 'oscillator' mouse; GlyR, glycine receptor; INL, inner nuclear layer; IPL, inner plexiform layer; MA, medium field amacrine; NF, narrowfield amacrine cell; PA, polyaxonal amacrine cell; S1–S5, sublamina 1–sublamina 5; WA, widefield amacrine cell.

Amacrine cells are the inhibitory interneurons of the inner retina. They receive synaptic input from bipolar and other amacrine cells and provide synaptic output onto bipolar, amacrine and ganglion cells. They represent the most diverse group of retinal neurons and comprise more than 30 different morphological types (MacNeil & Masland, 1998; Badea & Nathans, 2004). Approximately half of the amacrine cells are glycinergic, narrowfield amacrine cells; their cell bodies are located in the inner nuclear layer (INL), their dendrites are more vertically oriented and they provide local interactions between the different strata of the IPL, such as between the ON- and the OFF-sublaminas (Pourcho & Goebel, 1985; Menger *et al.* 1998; Hsueh *et al.* 2008). The other half of the amacrine cells are GABAergic. Their cell bodies are also found in the inner half of the INL; however, they are sometimes displaced into the ganglion cell layer (GCL). GABAergic amacrine cells have medium sized or widefield dendritic trees. They are involved in lateral interactions across the retina, such as surround inhibition or generation of direction selective light responses.

Until now ~17 different GABA-ergic, amacrine cells have been identified in the mouse retina (Badea & Nathans, 2004; Lin & Masland, 2006; Pérez De Sevilla Müller *et al.* 2007). In the present study, we concentrate on characterizing glycine receptors (GlyRs) of displaced, GABAergic amacrine cells (Hughes & Wieniawa-Narkiewicz, 1980; Perry, 1981; Brandon, 1985;

DOI: 10.1113/jphysiol.2009.171207

Wässle *et al.* 1987*a*; Pérez De Sevilla Müller *et al.* 2007). These are widefield amacrine cells; narrowfield amacrine cells have been studied previously (Weiss *et al.* 2008). Some widefield amacrine cells, such as the starburst amacrine cells, occur as mirror-symmetrical pairs: OFF-starburst cells have their cell bodies in the INL and their dendrites form the outer stratum of processes in the IPL. ON-starburst cells have their cell bodies in the GCL and their dendrites form the inner stratum of processes in the IPL. Thus they are regularly displaced. Other widefield amacrine cells, such as the A17 cells of the cat retina or the serotonin-accumulating amacrine cells of the rabbit have their cell bodies preferentially in the INL, but some cell bodies are displaced or better misplaced into the GCL (Sandell & Masland, 1986; Wässle *et al.* 1987*a*,*b*). The widefield amacrine cells in the GCL of the mouse retina have been systematically studied by Pérez de Sevilla Müller *et al.* (2007). They injected the cells with fluorescent dyes in retinal whole mounts and identified 10 different types based on their dendritic field sizes, horizontal and vertical stratification patterns, and general morphology. Starburst and A17 cells were amongst the 10 cell types encountered in that study.

The glycine receptor (GlyR) is a pentameric ligand-gated chloride channel. It is composed either of only α subunits (extrasynaptic GlyRs, reviewed by Betz & Laube, 2006), or of two α and three β subunits (synaptic GlyRs, Grudzinska *et al.* 2005). Four isoforms of the GlyRα subunit ($\alpha1$, $\alpha2$, $\alpha3$ and $\alpha4$) have been identified in mammals and, with alternative splicing, further diversity is possible (for review see Legendre, 2001; Lynch, 2004; Betz & Laube, 2006). In contrast, only a single GlyRβ subunit has been found. GlyRs are concentrated at synaptic sites through the interaction of the β-subunit with gephyrin, a scaffolding protein which aggregates GlyRs and links them to the cytoskeleton (for review see Kneussel & Betz, 2000). The presence of the β-subunit can thus be used as a reliable marker for synaptically localized GlyR isoforms. The physiological properties of neurons containing synaptic $\alpha1\beta$ and $\alpha2\beta$ GlyRs could be studied in the brainstem and spinal cord, because there is a postnatal switch from neonatal $\alpha2\beta$ to adult $\alpha1\beta$ receptors (Becker *et al.* 1988; Malosio *et al.* 1991; Takahashi *et al.* 1992; Singer *et al.* 1998; Smith *et al.* 2000). Concomitant with this switch, the mean decay time constant of neonatal GlyRs ($\tau = 14.2$ ms) becomes faster in adult GlyRs ($\tau = 6.7$ ms, Singer *et al.* 1998). However, synapses expressing the $\alpha3\beta$ or $\alpha4\beta$ have not been studied physiologically in the brainstem or spinal cord.

All four GlyRα subunits have been localized immunocytochemically at synapses in the IPL of the mouse retina (Haverkamp *et al.* 2003, 2004; Heinze *et al.* 2007). Most retinal glycinergic synapses contained only a single type of α subunit, however, the $\alpha2$ and $\alpha4$ subunits were co-localized in 31.5%, and the $\alpha2$ and $\alpha3$ subunit were co-localized in 26.7% of the respective synapses.

Synaptic GlyRs have also been studied by physiological means in the rodent retina by measuring spontaneous inhibitory postsynaptic currents (sIPSCs; Protti *et al.* 1997; Tian *et al.* 1998; Frech *et al.* 2001; Cui *et al.* 2003; Pérez-Leon *et al.* 2003; Eggers & Lukasiewicz, 2006; Gill *et al.* 2006; Ivanova *et al.* 2006; Majumdar *et al.* 2007; Veruki *et al.* 2007; Weiss *et al.* 2008). These studies showed that neurons involved with the fast transmission of light signals through the retina express GlyRs with fast kinetics, while neurons which occupy a more modulatory role express GlyRs with slower kinetics. More recently, glycine activated currents and sIPSCs were recorded both in wild-type mice and in mice deficient in GlyRα subunits (*Glra1*$^{spd\text{-}ot}$; *Glra3*$^{-/-}$; *Glra2*$^{-/-}$). It was found that bipolar cells express exclusively sIPSCs that were based on synaptic $\alpha1\beta$ GlyRs (Ivanova *et al.* 2006). In contrast, sIPSCs recorded from AII amacrine cells were based on synaptic $\alpha3\beta$ GlyRs and sIPSCs of narrowfield (NF) amacrine cells were mainly contributed by synaptic $\alpha2\beta$ GlyRs (Weiss *et al.* 2008). Veruki *et al.* (2007) have studied GlyRs of widefield amacrine cells of the rat retina and observed preferentially sIPSCs with slow kinetics. However, these authors could not study which subunits are responsible for such slow kinetics.

In the present study, the glycinergic input of displaced, widefield amacrine cells was characterized in whole mounts of the mouse retina. The cells were identified morphologically by the injection of a fluorescent tracer. Since it has been shown by immunocytochemistry that ON-starburst (cholinergic) amacrine cells express synaptic $\alpha4\beta$ GlyRs (Heinze *et al.* 2007) this cell type was studied in detail. Glycine induced currents and sIPSCs were recorded in wild-type mice and mice with specific GlyRα subunit deletions (*Glra1*$^{spd\text{-}ot}$, *Glra2*$^{-/-}$, *Glra3*$^{-/-}$). The kinetics of sIPSCs in wild-type and mutant mice were compared. It was found that morphologically distinct displaced widefield amacrine cells express GlyRs with different subunit compositions, and evidence is presented that synaptic, $\alpha4\beta$ GlyRs have very slow kinetics.

Methods

Preparation of retinal whole mounts, visualization and identification of the displaced amacrine cells

All procedures were approved by the local animal care committee and were in accordance with the law for animal experiments issued by the German Government (Tierschutzgesetz). Adult wild-type (C57BL/6J) mice and three transgenic mouse lines were used for the experiments. The transgenic mouse line *Glra3*$^{-/-}$ has a deletion in the gene coding for the GlyR$\alpha3$ subunit and expresses no functional $\alpha3$ subunit (Haverkamp *et al.*

2003, Harvey *et al.* 2004). The genetic status of each mouse used in the experiments was verified by polymerase chain reactions (PCR, for details see Harvey *et al.* 2004). The transgenic mouse line $Glra2^{-/-}$ carries a deletion mutation in the *Glra2* gene and expresses no functional $\alpha 2$ subunit. The $Glra2^{-/-}$ mouse line was generated by Lexicon Genetics (The Woodlands, TX, USA) by replacement of *Glra2* exon 1 with a LacZ/neo cassette via homologous recombination in embryonic stem cells. Positive clones were subsequently used to generate a mouse line containing this genetic alteration (Weiss *et al.* 2008). Another $Glra2^{-/-}$ mouse line has been characterized and described by Young-Pearse *et al.* (2006). Wild-type, $Glra3^{-/-}$ and $Glra2^{-/-}$ mouse lines have similar life expectancies and were studied at the early adult stages (5–8 weeks old). We also used the mouse mutant $Glra1^{spd\text{-}ot}$ (oscillator). At 3 weeks of age, homozygous $Glra1^{spd\text{-}ot}$ mice show prolonged periods of rapid tremor, producing extreme rigor and stiffness, and normally die around this time. This is due to a complete loss of the GlyRα1 subunit and results from a microdeletion of seven nucleotides within exon 8 of *Glra1* gene (Buckwalter *et al.* 1994, Kling *et al.* 1997). Juvenile $Glra1^{spd\text{-}ot}$ mice, of age 16–18 days, were used for the experiments. In control experiments, we also recorded from wild-type mice of the same age (16–18 days).

The mice were deeply anaesthetized with isoflurane (CuraMED Pharma GmbH, Karlsruhe, Germany) and decapitated. Retinas were dissected free of the eye cup in carbogen-bubbled (95% O_2–5% CO_2) Ames solution (Sigma-Aldrich, Taufkirchen, Germany) and mounted onto the experiment chamber with ganglion cell layer up. The cells were viewed by normal light illumination using differential interference contrast (Dodt & Zieglgänsberger, 1990) with a water immersion objective (63×, Zeiss, Oberkochen, Germany) on a fixed stage, upright microscope (Axioskop, Zeiss).

The experiments were done under laboratory light conditions, and consequently the retina was light-adapted. In general, to record from displaced amacrine cells, the cells with smallest soma size (8–10 μm diameter) were chosen. With a glass pipette, the inner limiting membrane on top of the soma was cut and removed, by gently pulling the membrane with the pipette and slightly tapping at the end of the headstage. This process was repeated several times until the soma and the area close to it was reasonably exposed. Occasionally, before the retina was mounted into the recording chamber, it was spread onto a Millipore filter paper (Schleicher and Schuell, NC10, Dassel, Germany), ganglion cell layer down, and was given gentle suction from beneath. The retina was then immediately dislodged from the filter paper by gentle brushing and mounted into the recording chamber with the ganglion cell layer up. This procedure allowed faster removal of the inner limiting membrane at the later stage.

Solutions and chemicals

The recording chamber was superfused at a rate of $\sim$2 ml min^{-1} with sodium bicarbonate-buffered Ames solution bubbled with carbogen. The solution contained (in mM): NaCl 120, KCl 3, $NaHCO_3$ 23, $CaCl_2$ 1.2, $MgSO_4$ 1.2, KH_2PO_4 0.5, D-glucose 6, amino acids, vitamins, pH 7.4. The intracellular solution contained (in mM): caesium gluconate 125, $CaCl_2$ 1, EGTA 10, $MgSO_4$ 4.6, Na-Hepes 10, Na-ATP 4, Na-GTP 0.4, QX-314 (a lidocaine derivative; Sigma-Aldrich, Taufkirchen, Germany) 5, Neurobiotin (Vector Laboratories, Burlingame, CA, USA) 15, Alexa 568 (Molecular Probes, Göttingen, Germany) 0.1, pH 7.3 adjusted with 5.9 M CsOH. All transmitter agonists and antagonists were applied by local superfusion through a multibarrel, pressure driven system (DAD12, ALA Scientific Instruments, Lambrecht, Germany) with a final common outlet (diameter 200 μm). The tip was placed within 100 μm from the cell soma. In preliminary experiments it was measured whether the superfusion system flushes the drugs over the whole widefield cell. Currents elicited by the application system did not change significantly if the outlet tube was moved further away from the cell soma in either direction. This indicates that dendritic fields of widefield amacrine cells were reasonably superfused. Hepes buffered solution was used in the DAD application system (in mM): NaCl 145, KCl 3.1, $CaCl_2$ 3, $MgCl_2$ 1.2, Na-Hepes 5, pH 7.4 adjusted with 1 M NaOH. For brevity, it will be called DAD solution in the following text. The Ca^{2+} concentration in the DAD solution was kept higher than that in the extracellular solution, to facilitate glycine release from the small field amacrine cells. Puffing control solution alone did not evoke any current. The estimated chloride equilibrium potential, at the room temperature (25°C), under the recording conditions was −51.5 mV (calculated between the intracellular and Ames solutions) and −57.0 mV (calculated between the intracellular and DAD solutions). The cation equilibrium potential lies between 0 mV (calculated between intracellular and Ames solutions) and 2 mV (calculated between intracellular and DAD solutions). The liquid junction potential of the Ames solution, with respect to the pipette solution, was approximately 15 mV (Liquid Junction Potential Calculator; Barry, 1994). The holding potential was corrected offline for the liquid junction potential.

The drugs were prepared as concentrated aliquots and stored at −20°C: glycine 100 mM (in DAD solution), GABA 100 mM (in water), gabazine 1 mM (in water), strychnine 5 mM (in water). Glycine was from Tocris (Biotrend Chemikalien GmbH, Köln, Germany); GABA, gabazine and strychnine were from Sigma-Aldrich (Taufkirchen, Germany). For each experiment, the stock solutions were freshly diluted in filtered DAD solution.

Patch-clamp recordings

The recordings were carried out at room temperature with an EPC-9 patch-clamp amplifier (HEKA Elektronik, Lambrecht, Germany) and Pulse 8.11 software. The patch pipettes were pulled from borosilicate glass tubing (Hilgenberg, Malsfeld, Germany). When filled with internal solution, they had a resistance of 5–8 MΩ. Cells were voltage-clamped in the whole-cell patch-clamp mode. Input resistances were 100–200 MΩ. Series resistances were ∼20 MΩ and were left uncompensated in most of the recordings. The cell and pipette capacitances were cancelled. The signals were filtered using the eight-pole Bessel filter built into the EPC-9 amplifier and digitized at a frequency at least twice the filter cut-off frequency. The sampling rate during the synaptic current recordings was 5 kHz; in the experiments with exogenous application of GABA and glycine, it was 2–5 kHz.

Experimental protocols and data analysis

The membrane potential of the cells was clamped to −5 mV, so that the directions of sIPSC and EPSC are opposite to each other. However, the driving force for Cl^- ions was 10 times that of cations and consequently inhibitory currents were enhanced. Glycine was applied for 3 s during exogenous application. Between applications, control solution was applied for 2 min allowing GlyRs to recover. For a more detailed analysis of GlyRs, glycinergic sIPSCs were recorded in the presence of the GABA-A receptor antagonist gabazine. Later, the identity of the glycinergic sIPSCs was confirmed by blockade with a mixture of gabazine and strychnine. Glycinergic sIPSCs were quantified using the MiniAnalysis software (Synaptosoft, Leonia, NJ, USA). Each detected event was individually inspected and only outward going events (chloride current) were chosen for analysis. Well separated events, that did not show any signs of multiple peaks, were selected for analysis. Frequencies, peak amplitudes, the exponential decay time constants and the rise times (10%–90%) were measured. Decay time constants (decay τ) were determined by a least-square fit of 10–90% of the decay phase, using a single exponential decay function. A single exponential fit was sufficient for describing the decay kinetics of sIPSCs in all the cells recorded in this study. A χ^2 analysis based method was used to compare the fits. For each cell, histograms of the frequency of the decay time constants were calculated and normalized. Finally, the histograms of all the cells of a particular type were added together and normalized once again. This procedure was invariant with respect to the total number of events recorded from individual cells. Plotting the individual events from the same cells without normalization procedure yielded similar results. The data showing glycine evoked response (Fig. 2*C*) are presented as means ± S.E.M. (standard error of the mean). Statistical analyses were performed using Student's two-tailed *t*-test (unpaired, for two groups). Differences were considered to be significant at the $P < 0.05$ level. For the frequency distributions of decay time constants (Figs 3–5) means ± S.D. (standard deviation) were calculated. To determine whether the distributions of the decay time constants are significantly different, the Kolmogorov–Smirnov test (for two datasets) was used and the differences were considered significant at the $P < 0.01$ level. The number of cells used for the analysis is indicated as '*n*', the total number of sIPSCs is labelled as '*N*'. Glycinergic sIPSCs, used for analysis, were recorded before the application of strychnine.

Immunocytochemical staining of displaced amacrine cells

After the patch-clamp recordings, the retinal whole mounts, with Alexa 568 and neurobiotin filled cells, were fixed for 12–15 min with 4% paraformaldehyde in 0.1 M phosphate buffer (PB) at room temperature and washed in PB several times. The retinas were incubated in 5% Chemiblocker (membrane-blocking agent, non-animal protein blocker, Chemicon, Hofheim, Germany), 1% Triton X-100 in PB with Streptavidin Alexa 568 (1 : 1000; Molecular Probes, Göttingen, Germany), either at 4°C for 2 days or at room temperature for 3 h. Both incubation methods gave equivalent results. The retinas were washed in PB several times and confocal photomicrographs were taken with a Zeiss LSM 5 Pascal confocal microscope using a 40× oil immersion objective. Stacks of confocal images (z-stack step size 0.6 μm) were projected onto a single image plane. The size and contrast of the images were adjusted using Adobe Photoshop CS.

Immunocytochemistry of GlyRs of displaced widefield amacrine cells

To examine glycine receptor expression of displaced amacrine cells by immunocytochemical staining with subunit specific antibodies, the retinas used for patch clamp recordings were fixed in 4% PFA for 8 min. In some cases a different fixation protocol was applied, using 4% (w/v) carbodiimide in PB. In those cases, the retinas were mounted onto nitrocellulose filters and immersion fixed for 25 min. The retinal whole mount preparations were washed several times in PB, before and immediately after immunocytochemical reactions with primary and secondary antibodies.

Antibodies

In the present study, the GlyRα2 subunit was visualized by a goat polyclonal antiserum against the 18 N-terminal amino acids of the human GlyRα2 subunit (dilution 1 : 300, Santa Cruz Biotechnology, GlyRα2 [N-18]: SC-17279). Its specificity has in a previous study been tested on HEK 293T cells transfected with expression constructs for GlyRα1, GlyRα2, GlyRα3 and GlyRα4 (Haverkamp *et al.* 2004). No specific staining was observed in *Glra2*$^{-/-}$ mouse retinas (Weiss *et al.* 2008).

Labelling of the GlyRα4 subunit was achieved by using a rabbit polyclonal antiserum raised against the 14 C-terminal amino acids of the mouse GlyRα4 subunit (dilution 1 : 500). The generation, purification and specificity of the antiserum have in detail been described in a preceding study (Heinze *et al.* 2007).

Immunohistochemistry protocol

The antibodies were diluted in 0.1 M PB containing 5% Chemiblocker (Chemicon) and 1% Triton X-100. Immunocytochemical labelling was performed using the indirect fluorescence method. The retinal whole mounts were incubated freely floating overnight in a mixture a primary antibodies, followed by 3 h incubation in a mixture of secondary antibodies which were conjugated either to Alexa 488 (green fluorescence; Molecular Probes, Eugene, OR, USA) or to CY3 (red fluorescence; Dianova, Hamburg, Germany) and streptavidin conjugated to Alexa 488 or Alexa 568.

Light microscopy

Confocal photomicrographs were taken by using a Zeiss LSM 5 Pascal confocal microscope equipped with an argon and a HeNe laser. High-resolution scanning was performed with a Plan-Apochromat 63×/1.4 objective and with 1024 × 1024 or 2048 × 2048 pixels. The brightness and the contrast of the final images were adjusted using Adobe Photoshop CS2. Photomicrographs were taken as single optical sections or as z-axis stacks of 20 single optical sections (step size 0.2 μm).

Results

Morphological identification of displaced widefield amacrine cells

Displaced amacrine cells could be easily distinguished from the ganglion cells in the GCL as they have the smallest cell bodies (~8–10 μm). Physiologically, it was often difficult to distinguish a ganglion cell from a displaced amacrine cell because many widefield amacrine cells drive action potentials. During the whole cell recordings each cell was filled with Alexa 568 and neurobiotin and later counterstained with streptavidin to reveal their morphology. The widefield amacrine cells were classified into 11 types following their most recent description by Pérez De Sevilla Müller and colleagues (2007). Starburst cells (Fig. 1*A*) were most frequently encountered and could be recognized from their typical radiate morphology. Three other medium-field amacrine cells (MA) were distinguished from the stratification of their dendrites in sublamina S1–S5 (Fig. 1*B*, *C* and *D*). A17 cells were also routinely encountered and because of their thin, radiate and varicose dendrites they could be clearly recognized (Fig. 1*E*). Three polyaxonal amacrine cells (PA) were also identified according to the stratification of the dendrites and axons in specific sublaminas of the IPL (Fig. 1*F*, *G* and *I*). The axons of PA-amacrine cells did not run to the optic nerve head but projected diffusely into the IPL. Finally three types of widefield amacrine cells (WA) were routinely encountered (Fig. 1*H*, *J* and *K*). The dendrites of most of these cells extend beyond the window size in Fig. 1. None of the cells used in this study projected any of their dendrites/axons to the optic nerve head. Also the dendritic/axonal processes were always found in the IPL; none were found in the optic nerve fibre layer. Hence the question of confusing the cells with ganglion cells did not arise. Badly filled cells were not incorporated in the study. The morphology of the cells was individually examined using the confocal microscope before assigning a name to them.

Response of widefield amacrine cells to the application of glycine

When exogeneous glycine (10 mM in the drug pipette) was applied for 3 s to the retina of wild-type mice, Cl^--based outward currents were elicited in all 11 displaced amacrine cell types (Fig. 2). The amplitudes varied from 400 pA to 700 pA and the currents were suppressed by strychnine (3 μM, applied from the puffer pipette). Figure 2*A* and *B* shows the currents elicited in an A17 and a starburst amacrine cell. Glycine was also applied to displaced amacrine cells in the three mutant mouse lines *Glra3*$^{-/-}$, *Glra2*$^{-/-}$ and *Glra1*$^{spd\text{-}ot}$. No significant differences, when compared to wild-type mouse responses were observed in *Glra3*$^{-/-}$ and *Glra1*$^{spd\text{-}ot}$ mice (Fig. 2*C*). Very low amplitude or no glycine induced currents were found for cell types PA-S4, WA-S3 and WA-multi in the case of *Glra2*$^{-/-}$ mice. This statistically significant, nearly complete absence of glycine induced currents suggests, that the GlyRα2 subunit is a major constituent of the GlyRs expressed by these three cell types. Statistically significant reduction in the glycine evoked current was also observed for the starburst and MA-S5 cells in *Glra2*$^{-/-}$ mice, although a residual glycine induced current of moderate

amplitude persisted. Both in wild-type and in mutant mice all displaced amacrine cells responded to the application of GABA (200 μM, not shown).

The morphological classification of the cells was first performed on the microscope by inspection. The level of stratification was determined from confocal stacks through the inner plexiform layer. A quantitative morphometric analysis or a cluster analysis was not performed. No obvious morphological differences were observed between the types of widefield amacrine cells recorded and stained in wild-type mice and in the three mutant mouse lines. The individual displaced amacrine cell types were targeted with the patch electrode without pre-labelling, and recording a given type was just by chance. In addition, recordings from wild-type and three mutant mice had to be compared. Some of the cells, such as starburst cells, were recorded frequently, some only rarely. The encounter frequencies of each type of widefield amacrine cell are indicated at the bottom of Fig. 2*C*. To get sufficient data for the following analysis of spontaneous inhibitory postsynaptic currents (sIPSCs) we pooled cells into three major groups, based on the results of exogenous application of glycine and the encounter frequency of sIPSCs in *Glra2*$^{-/-}$ mice. Group I comprises the cells which responded to the exogenous application of glycine with a moderate to high amplitude outward current and showed spontaneous sIPSCs in wild-type and all mutant mice (MA-S5, MA-S1, MA-S1/S5, A17, PA-S5,

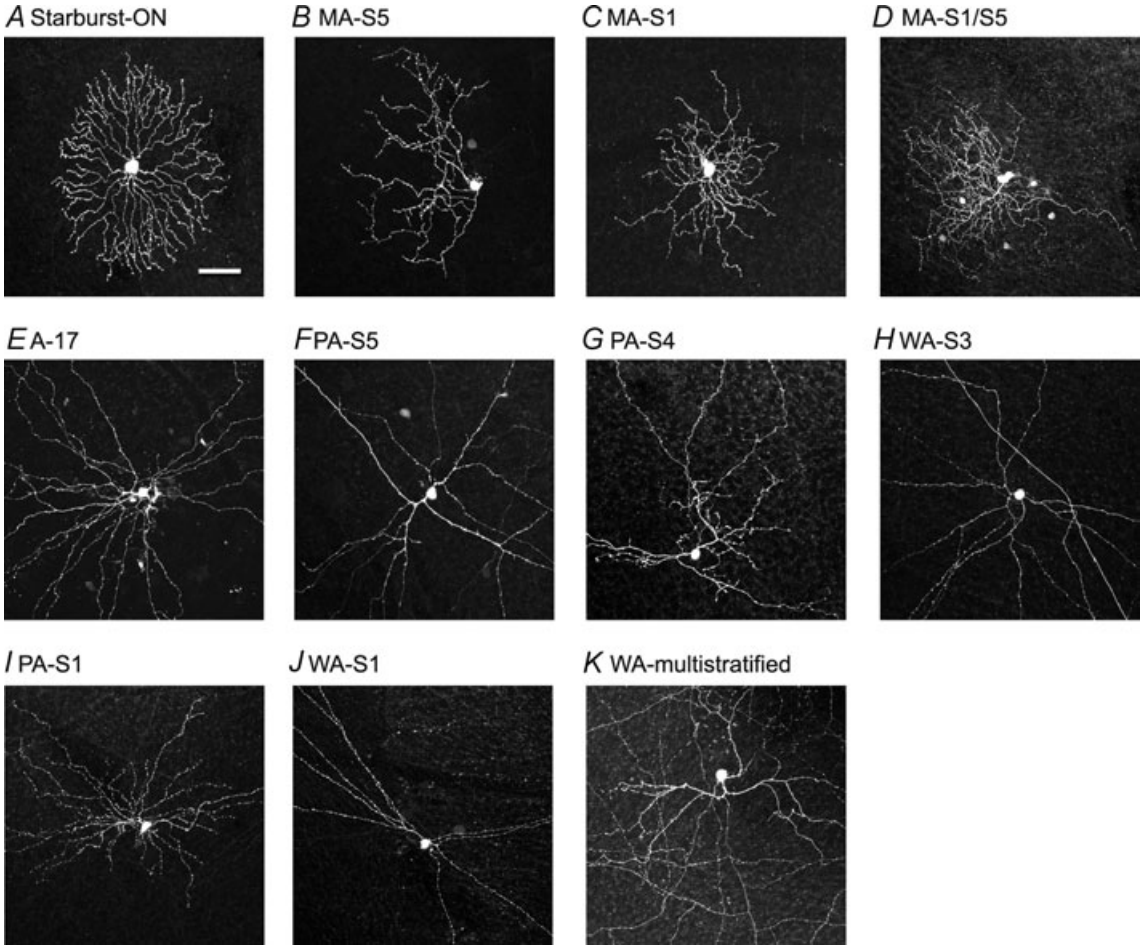

Figure 1. Morphological identification of 11 displaced amacrine cell types following whole cell recordings and intracellular filling with Alexa 568 and neurobiotin
The horizontal view is shown (collapsed stack of confocal sections). The z-axis of the confocal sections was carefully studied to assess the stratification level of each cell's dendritic arbor. The morphological classification followed the nomenclature of Pérez De Sevilla Müller *et al.* (2007). *A*, starburst (cholinergic) amacrine cell. *B*, mediumfield amacrine cell stratifying in sublamina S5 (MA-S5). *C*, mediumfield amacrine cell stratifying in S1 (MA-S1). *D*, mediumfield amacrine cell stratifying in S1 and S5 (MA-S1/S5). *E*, A17 amacrine cell. *F*, polyaxonal amacrine cell stratifying in S5 (PA-S5). *G*, polyaxonal amacrine cell stratifying in S4 (PA-S4). *H*, widefield amacrine cell stratifying in S3 (WA-S3). *I*, polyaxonal amacrine cell stratifying in S1 (PA-S1). *J*, widefield amacrine cell stratifying in S1 (WA-S1). *K*, widefield amacrine cell with processes in different sublaminas (WA-multistratified). Scale bar: 50 μm.

PA-S1 and WA-S1). Group II comprises the cells which showed very small or no glycine induced currents and no sIPSCs in *Glra2*$^{-/-}$ mice (PA-S4, WA-S3 and WA-multi). Starburst amacrine cells were recorded frequently and thus formed the third group.

Recording of glycinergic spontaneous inhibitory postsynaptic currents (sIPSCs)

Many of the displaced widefield amacrine cells displayed spontaneous postsynaptic membrane current fluctuations. The spontaneous events were recorded at −5 mV holding potential (Fig 3*A* and *B*), a potential close to the cationic reversal potential (0 to 2 mV, see Methods), such that the excitatory events are very small in amplitude and opposite in sign with respect to the inhibitory events (Cl^- reversal potential between −51.5 and −57.0 mV, see Methods). The sIPSCs recorded in DAD (control) solution is shown in Fig. 3*Aa* and *Ba* for WA-S3 and A17 cells, respectively. The glycinergic sIPSCs were isolated using 3 μM gabazine. The drug was puffed very close to the cell for 1 min during which the spontaneous events were recorded. However, application of gabazine, a general GABA-A receptor blocker, causes strong disinhibition in the whole retina giving rise to large inhibitory membrane current jumps (Fig. 3*Ab* and *Bb*). To reduce this disinhibitory effect, we applied 20 μM APB, a metabotropic glutamate receptor agonist, to selectively block the ON pathway in the retina. This procedure reduced the large baseline membrane current oscillations and helped in isolating individual sIPSC events (Fig. 3*Ac* and *Bc*). Strychnine at 3 μM was applied in conjunction with 3 μM gabazine (Fig. 3*Ad* and *Bd*) to confirm the glycinergic nature of sIPSCs recorded in panels *b* and *c*. Figure 3*C* shows the glycinergic sIPSCs of an A17 amacrine cell (Fig. 3*B*) at higher temporal resolution. For well separated events the 10–90% decay phase was analysed to assess the decay time constant (decay τ) using a mono-exponential fitting algorithm in-built in the Mini-Analysis software. Figure 3*D* shows one such fitting result

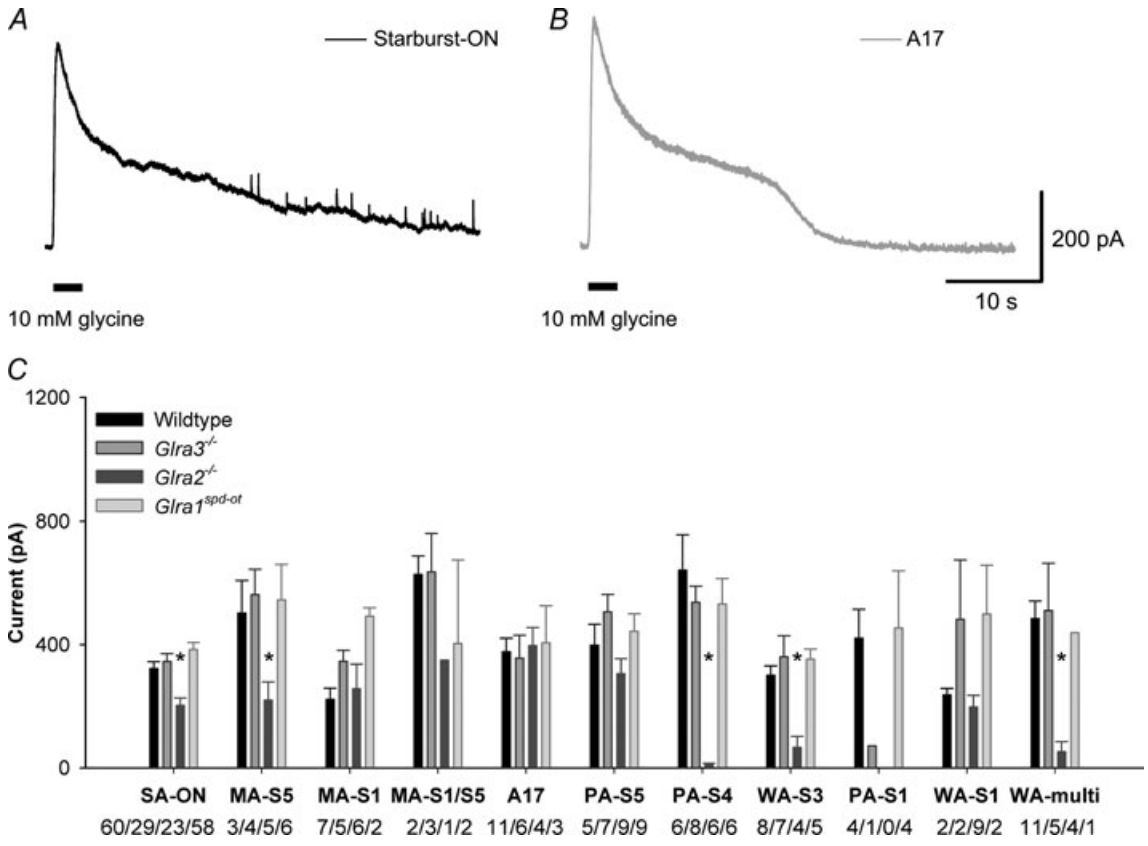

Figure 2. Glycine induced outward currents recorded from the 11 different types of amacrine cells described in Fig. 1

Glycine was applied for 3 s at a concentration of 10 mM in the puffer pipette. The cells were voltage clamped at $V_H = -5$ mV. *A*, glycine evoked current recorded from a starburst amacrine cell. *B*, glycine induced current evoked from an A17 amacrine cell. *C*, results from wild-type, *Glra3*$^{-/-}$, *Glra2*$^{-/-}$ and *Glra*$^{spd\text{-}ot}$ mice are compared. The data are presented as means ± S.E.M. *Statistically different at $P < 0.05$ significance level. The numbers underneath the cell types represent the encounter frequencies of the cells in the wild-type and the three mutant mice.

(black curve) for an averaged sIPSC (grey curve) recorded from the cell presented in Fig. 3*B*. Figure 3*E* shows the normalized decay τ distribution measured from the cell presented in Fig. 3*B*.

Distribution of decay time constants τ of glycinergic sIPSCs

Figure 4*A*, *C*, *E* and *G* represent the normalized decay time constant distributions of group I widefield amacrine cells in wild-type, *Glra3*$^{-/-}$, *Glra1*$^{spd\text{-}ot}$ and *Glra2*$^{-/-}$ mice, respectively. Each distribution shows a characteristic peak around 5–8 ms and a very broad tail spanning up to 150 ms. The mean τ values are: wild-type: 23.8 ± 8.9 ms; *Glra3*$^{-/-}$: 24.1 ± 8.8 ms; *Glra1*$^{spd\text{-}ot}$: 25.6 ± 10.5 ms; and *Glra2*$^{-/-}$: 26.7 ± 6.9 ms. Similarly, normalized τ distributions of glycinergic sIPSCs are shown for group II widefield amacrine cell in Fig. 4*B*, *D* and *F*, representing data from wild-type, *Glra3*$^{-/-}$ and *Glra1*$^{spd\text{-}ot}$ mice, respectively. In group II cells recorded from the retinas of *Glra2*$^{-/-}$ mice no glycinergic sIPSCs could be encountered. The mean decay time contants, τ, are: wild-type: 26.8 ± 9.8 ms; *Glra3*$^{-/-}$: 23.4 ± 10.3 ms; *Glra1*$^{spd\text{-}ot}$: 31.5 ± 8.8 ms.

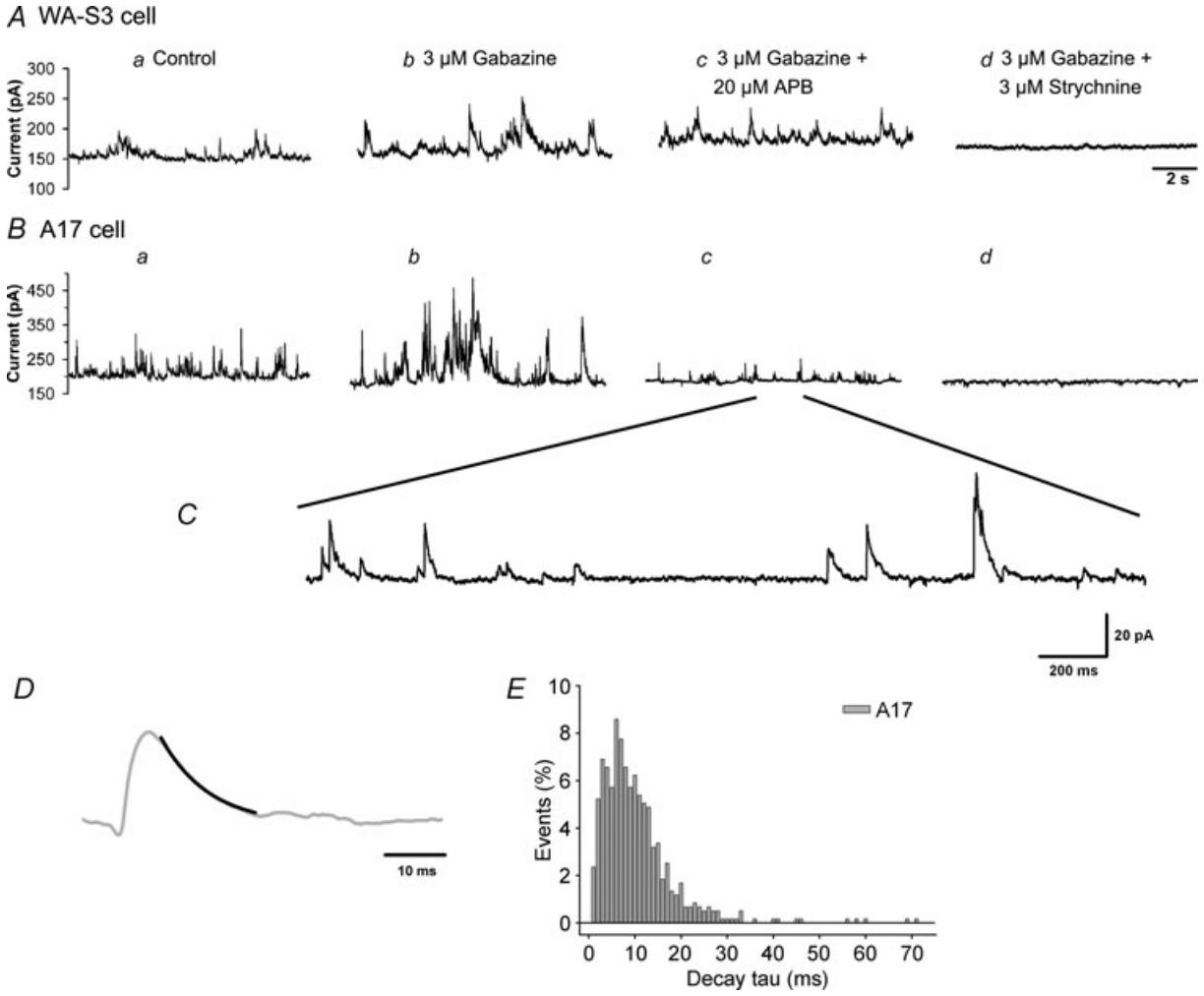

Figure 3. Analysis of spontaneous inhibitory postsynaptic currents (sIPSCs)
A, recordings from a WA-S3 cell ($V_H = -5$ mV). The sIPSCs were recorded in control solution (*a*), in the presence of 3 μM gabazine (*b*), in the presence of 3 μM gabazine and 20 μM APB (*c*) and in the presence of 3 μM gabazine and 3 μM strychnine (*d*). *B*, recordings from an A17 cell (conventions as in *A*). *C*, the sIPSCs recorded from the A17 cell in the presence of 3 μM gabazine and 20 μM APB are shown at higher magnification. Individual well-isolated sIPSCs were chosen to measure the amplitude, the 10–90% rise time and the decay time constant τ (measured from the 90–10% decay curve). *D*, mono-exponential fit to the decay phase of an average sIPSC recorded from the A17 cell in *B*. *E*, histogram of the decay time constants τ measured from the A17 cell in *B*.

Distributions of the decay time constants τ of starburst amacrine cells

Since we were able to record sufficient numbers of ON-starburst cells both in wild-type and mutant mice, they are presented as a seperate group here. However, recordings from ON-starburst cells were hampered by two difficulties. It is possible that at rest ON-starburst cells receive a tonic glycinergic input. Application of strychnine elicited an inward current in these cells, possibly by blocking the action of endogenous glycine (data not shown). For that reason it is possible that the glycinergic

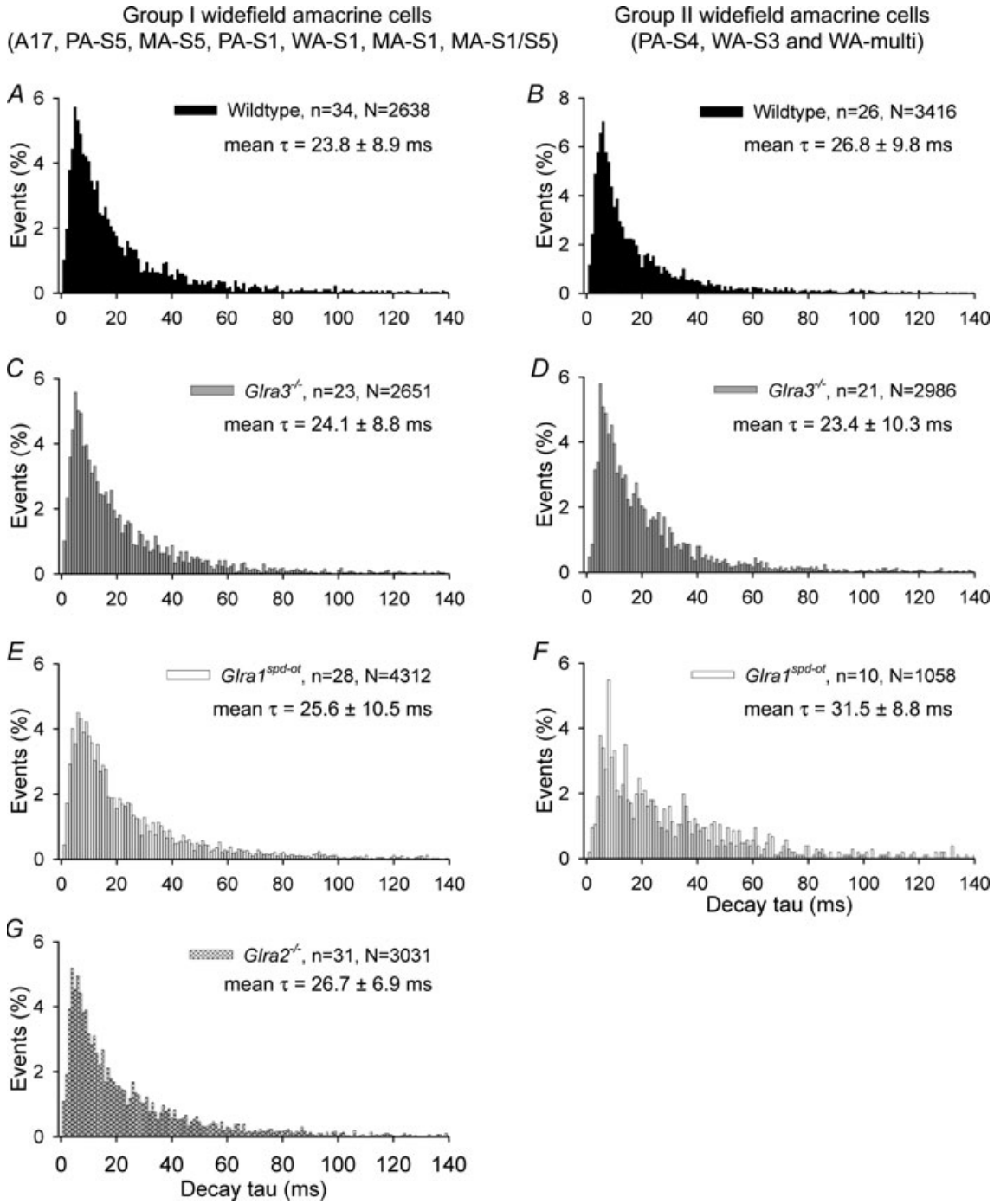

Figure 4. Comparison of the decay time constants, τ, of glycinergic sIPSCs obtained from group I and group II amacrine cells in wild-type and mutant mice
A and *B*, histograms of τ values measured in wild-type mice (*n*: number of cells; *N*: number of sIPSC analysed). *C* and *D*, histograms of τ values measured in *Glra3*$^{-/-}$ mice. *E* and *F*, histograms of τ values measured in *Glra1*$^{spd\text{-}ot}$ mice. *G*, histograms of τ values measured in *Glra2*$^{-/-}$ mice.

currents induced by exogenous application of glycine underestimate the total current. A second problem was the scarcity of glycinergic sIPSCs that could be recorded from ON-starburst cells, probably as a consequence of tonic glycinergic input. Few moderately fast glycinergic sIPSCs were found in some cells, although the majority of sIPSCs were slow (see online supplemental Fig. 1). However, since sufficient numbers of ON-starburst cells were recorded, representative histograms of decay time constants could be constructed. Figure 5 compares the sIPSCs recorded from

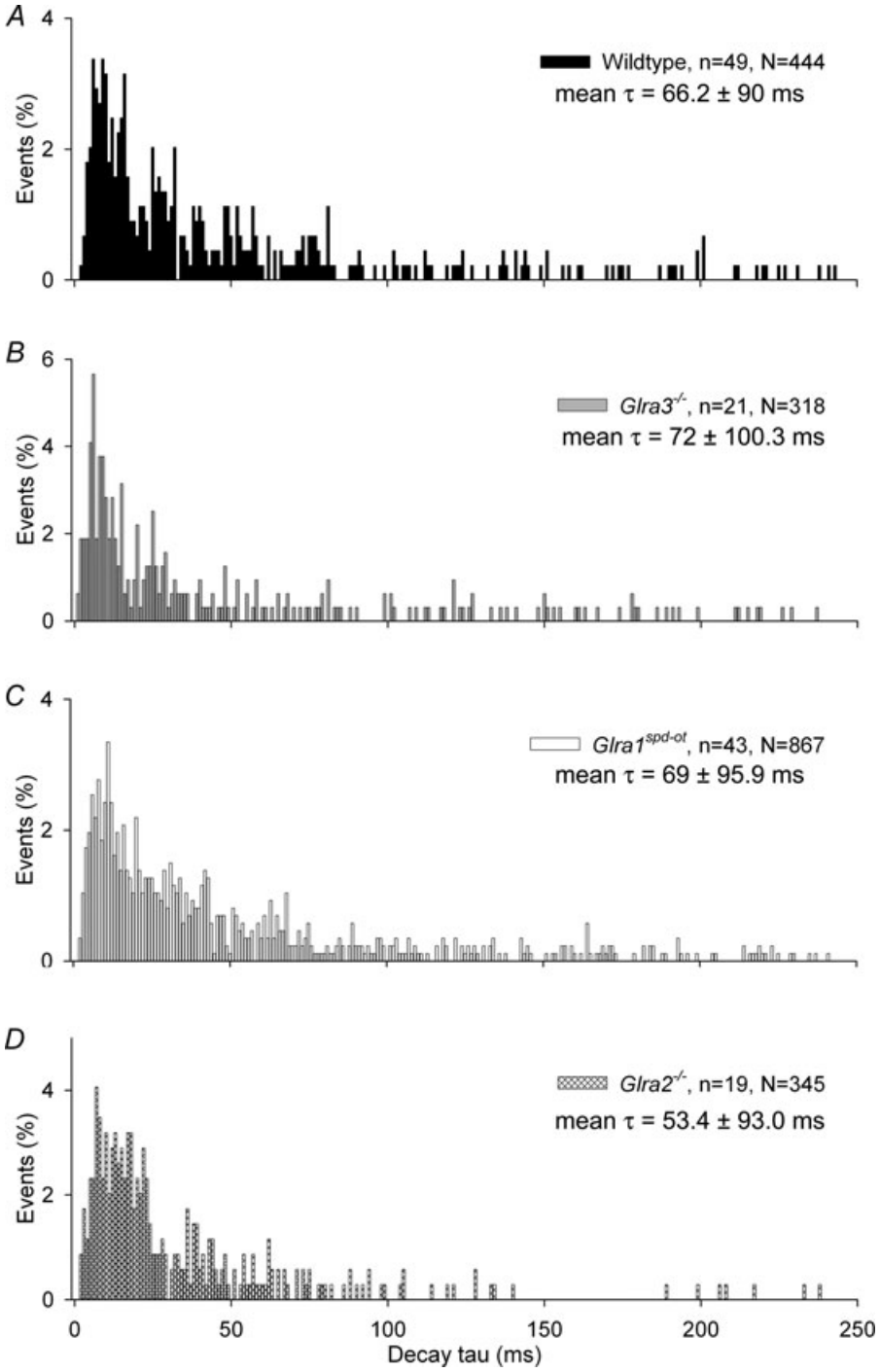

Figure 5. Comparison of the decay time constants, τ, of glycinergic sIPSCs obtained from starburst amacrine cells in wild-type and mutant mice
Histograms of the τ values measured in wild-type mice (*A*), *Glra3*$^{-/-}$ mice (*B*), *Glra1*$^{spd\text{-}ot}$ mice (*C*) and *Glra2*$^{-/-}$ mice (*D*).

ON-starburst cells in wild-type and the three mutant mice. There is not much difference between the distributions of decay time constants and their means are: 66.2 ± 90 ms (wild-type, Fig. 5*A*), 72 ± 100.3 ms (*Glra3*$^{-/-}$, Fig. 5*B*), 69 ± 95.9 ms (*Glra1*$^{spd\text{-}ot}$, Fig. 5*C*), and 53.4 ± 93.0 ms (*Glra2*$^{-/-}$, Fig. 5*D*).

Decay time constants and dendritic filtering

Scatter diagrams comparing the rise times and the event amplitudes of sIPSCs with their decay time constants were generated. Examples of such comparisons are shown in Fig. 6. No correlation was found (indicated by the black regression lines in each curve) between rise time and decay τ of starburst and WA-S3 cells (Fig. 6*A* and *C*, respectively). Similarly the event amplitudes and decay time constants were not correlated for starburst and WA-S3 cells (Fig. 6*B* and *D*, respectively). For other widefield amacrine cells too, no correlation was found between rise time and decay time constant, or between event amplitude and decay time constant. This indicates that dendritic filtering is not responsible for the long decay time constants of widefield amacrine cells. Scatter diagrams comparable to those shown in Fig. 6 were also drawn for the sIPSCs recorded from group I, group II and starburst amacrine cells in the mutant mice (not shown) and no correlations between decay τ and event amplitude or rise time were encountered. This demonstrated that the changes in the kinetics of decay time constants were not the result of dendritic filtering.

Comparison of decay time constants

The histograms in Fig. 4*A*–*F* were integrated and the resulting cumulative distributions are presented in Fig. 7*A* and *B*. Comparison of the cumulative frequencies of τ values of group I widefield amacrine cells measured in wild-type and the three mutant mice revealed no statistically significant difference ($P > 0.05$). Since the data of the *Glra1*$^{spd\text{-}ot}$ could be measured only in juvenile (P16–P18) mice, we have also inserted in Fig. 7*A* data from juvenile wild-type mice, which are not different from adult wild-type mice and juvenile *Glra1*$^{spd\text{-}ot}$ mice. There is no significant difference between wild-type and α2-knockout mice among group I widefield amacrine cells. This finding substantiates the conclusion that sIPSCs of group I cells are not dominantly shaped by α2 subunits.

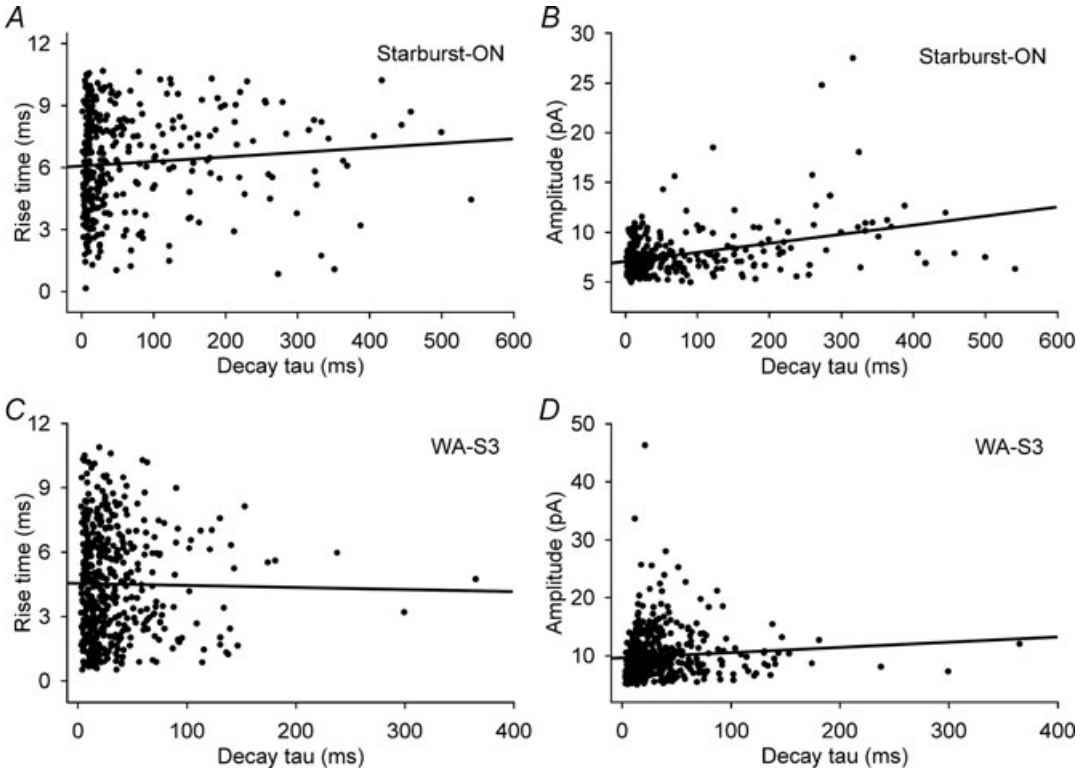

Figure 6. Scatter diagrams comparing decay time constants with rise times and sIPSC amplitudes
A and *C*, rise times of glycinergic sIPSCs are plotted against decay τ values for starburst and WA-S3 cells, respectively. *B* and *D*, event amplitudes of glycinergic sIPSCs are plotted against decay τ values for starburst and WA-S3 cells, respectively. In each curve, black straight line indicates the linear regression fit to the data.

The results of group II cells (Fig. 7*B*) are not as clear as those of group I cells. There is no significant difference between adult wild-type mice and *Glra3*$^{-/-}$ mice ($P > 0.05$). However, data of adult and juvenile wild-type mice are different: in juvenile wild-type mice there is a significant tendency for longer τ values ($P < 0.01$, Fig. 7*B*). In addition, there is also a significant prolongation of τ values in (juvenile) *Glra1*$^{spd\text{-}ot}$ mice, in comparison to juvenile wild-type mice ($P < 0.01$, Fig. 7*B*). However, in contrast to group I cells, no sIPSCs could be recorded from group II cells in α2 knockout mice. This finding supports the conclusion that sIPSCs of group II cells are dominated by α2 subunits. However a minority of glycinergic synapses of group II cells could be constituted by the fast conducting GlyRα1, whose deletion in the *Glra1*$^{spd\text{-}ot}$ mice causes slower sIPSCs.

The cumulative distributions of the decay time constants of starburst amacrine cells (Fig. 7*C*) show that, with the exception of the data from *Glra2*$^{-/-}$ mouse retina, all curves are very similar. Surprisingly, the decay time constant of the glycinergic sIPSCs of ON-starburst cells are apparently speeded up in *Glra2*$^{-/-}$ mice, indicating the presence of a slow conducting α2 subunit in the glycinergic synapses of starburst amacrine cell. This will be discussed in detail in the next section.

We also compare in Fig. 7*D* the decay time constants of glycinergic sIPSCs recorded in the present study for group I and group II widefield and ON-starburst amacrine cells with those of AII and other narrowfield (NF) amacrine cells measured in our preceding study (Weiss *et al.* 2008). The fastest glycinergic sIPSCs observed in amacrine cells were those of AII amacrine cells. The slowest sIPSCs were found in ON-starburst cells. The group I and group II widefield and the NF amacrine cells expressed GlyRs with intermediate decay time constants.

Immunocytochemical localization of GlyRα4 and GlyRα2 on widefield amacrine cells

In addition to the physiological measurements, we tried to immunocytochemically identify the GlyR expression

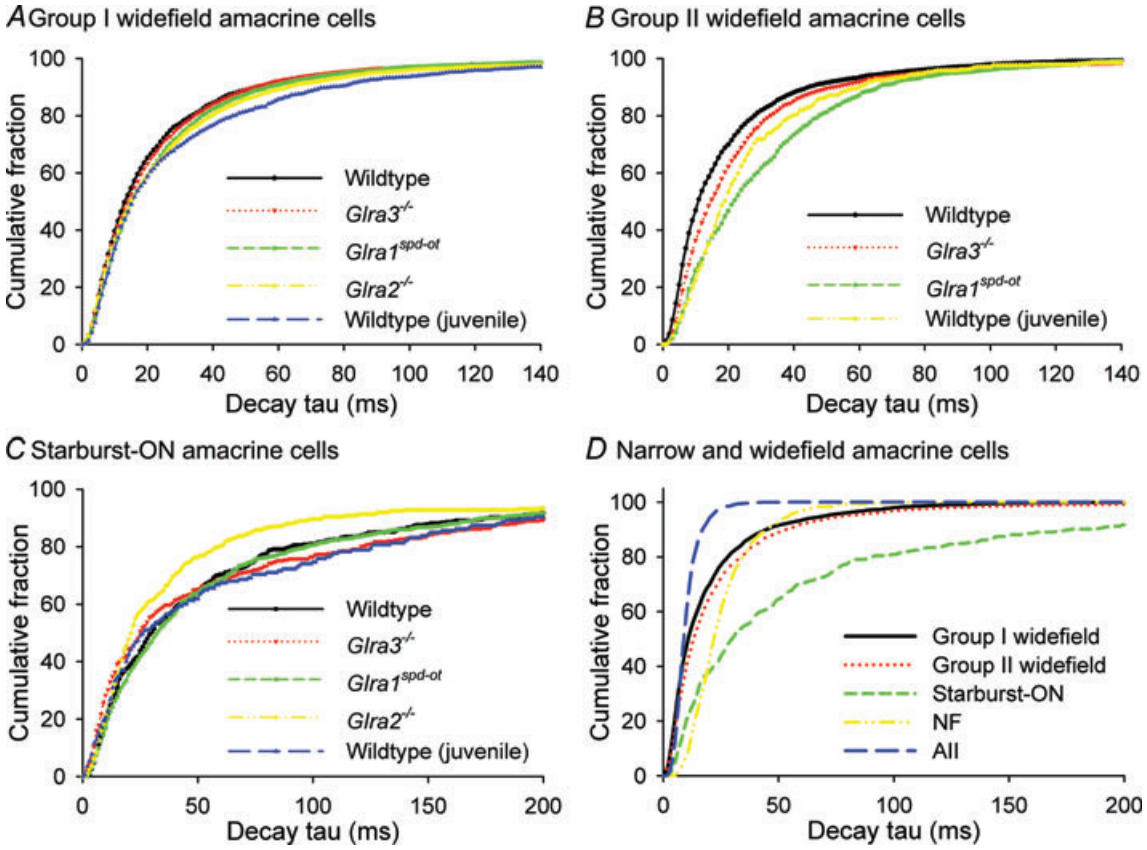

Figure 7. Cumulative frequency plots of decay time constants of group I (*A*) and group II (*B*) widefield amacrine cells
Results from wild-type (adult), wild-type (juvenile) and mutant mice are compared. *C*, cumulative frequency plot of decay time constants of starburst amacrine cells. *D*, cumulative frequency plot comparing the decay time constants of group I widefield, group II widefield and starburst amacrine cells with those of AII and narrowfield (NF) amacrine cells recorded in our preceding study (Weiss *et al.* 2008).

pattern of the displaced amacrine cells. The cells were filled with Alexa 568 and neurobiotin during recording. After the recording the retina was immunostained for the GlyRα4 and GlyRα2 subunits. We did not immunostain the retinas for the GlyRα1 and GlyRα3 subunits because in *Glra1*$^{spd-ot}$ and *Glra3*$^{-/-}$ mice we did not find any differences in the sIPSCs in comparison to wild-type mice. Therefore, these two subunits apparently are not very much involved in glycinergic signalling of widefield amacrine cells.

Figure 8*A* and *B* shows a typical group I (MA-S1) and a group II (PA-S4) cell. Single confocal sections of the fields indicated by the rectangles are shown at higher magnification in Fig. 8*Aa*, *Ab*, *Ba* and *Bb*. GlyRα4 immunoreactivity (green) is punctate, which represents, as has been previously shown by electron microscopy, synaptic localization (Sassoè-Pognetto *et al.* 1994). As indicated by the arrowheads, some GlyRα4 puncta coincide with the dendrites of these two widefield amacrine cells, suggesting these cells receive synapses expressing the GlyRα4 subunit.

We also immunostained a group I widefield amacrine cell (MA-S5) for the GlyRα2 subunit (Fig. 9*A*). The fields marked by the squares in Fig. 9*A* are shown at higher magnification as single confocal sections (Fig. 9*Aa* and *Ab*). GlyRα2 immunoreactive puncta are found on the dendrites of this cell. These results can be generalized: both GlyRα2 and GlyRα4 puncta were observed on many group I and group II widefield amacrine cells immunolabelled for these two subunits.

In a preceding study (Heinze *et al.* 2007) it has been shown that the density of GlyRα4 immunoreactive puncta is highest in the stratum where ON-starburst cell dendrites are found. An ON-starburst cell, injected with neurobiotin during electrophysiological recording, is shown in Fig. 9*B*. The cell was also immunolabelled for the GlyRα4 subunit and the squares indicated in Fig. 9*B* are shown at higher magnification in Fig. 9*B*a and *Bb*. As indicated by the arrowheads, many GlyRα4 immunoreactive puncta coincide with the dendritic varicosities of this cell. We also immunostained ON-starburst cells for the GlyRα2 subunit (not shown) and observed few immunoreactive puncta on the dendritic varicosities. The anatomical results suggest that group I, group II and starburst amacrine cells receive glycinergic synapses expressing the GlyRα2 and GlyRα4 subunits.

Discussion

Glycinergic, synaptic input of widefield amacrine cells

Spontaneous glycinergic IPSCs have been recorded in mammalian retinal slices, wholemounts and organotypic cultures (Protti *et al.* 1997; Tian *et al.* 1998; Frech *et al.* 2001; Cui *et al.* 2003; Pérez-León *et al.* 2003; Eggers & Lukasiewicz, 2006; Gill *et al.* 2006: Ivanova *et al.* 2006; Majumdar *et al.* 2007; Veruki *et al.* 2007; Weiss *et al.* 2008). There is a general tendency in these studies that retinal neurons involved with the fast, vertical transmission of light signals express GlyRs with fast kinetics. This holds true for bipolar cells, AII amacrine cells and A-type ganglion cells. Most amacrine cells, besides AII cells, are modulatory interneurons (Masland, 2001; Wässle, 2004) and the above studies have presented evidence that they express GlyR with slow kinetics. Frech *et al.* (2001) recorded glycinergic sIPSCs from four mouse amacrine cells of unknown type. The decay time constants of the glycinergic sIPSCs of the four cells could be approximated by a bi-exponential fit with a weighted decay time constant $\tau_w = 25.3 \pm 1.9$ ms. Veruki *et al.* (2007) studied the functional properties of GlyRs of widefield amacrine cells in the rat and observed a mean decay time constant of 26 ms, suggesting the expression of GlyRs with slow kinetics. Weiss *et al.* (2008) recorded glycinergic sIPSCs from narrowfield – non AII – amacrine cells of the mouse retina and observed a mean decay time constant $\tau = 27 \pm 6.8$ ms. In the present study we found for group I widefield amacrine cells a mean decay time constant $\tau = 23.8 \pm 8.9$ ms and for group II cells $\tau = 26.8 \pm 9.8$ ms, which is in close agreement with the results from rat widefield amacrine cells (Veruki *et al.* 2007).

Subunit composition of GlyRs of widefield amacrine cells

In the retina of the gephyrin knockout mouse all synaptic GlyR aggregates have disappeared (Fischer *et al.* 2000). Since gephyrin binds to the β subunit (Kneussel *et al.* 1999) this result implies that synaptic GlyRs of the retina are αβ heteromeric receptors. To date, selective agonists or antagonists that distinguish different isoforms of synaptic GlyRs have not been identified (Harvey & Betz, 2000; Legendre, 2001; Lynch, 2004; Betz & Laube, 2006). In the present study we investigated mice with specific deletions of GlyR subunits for the analysis of synaptic GlyRs of widefield amacrine cells. The clearest result can be expected if given retinal cell types express exclusively α1β, α2β or α3β synaptic receptors. In this case glycinergic sIPSCs with characteristic decay time constants should be present in wild-type mice, and both sIPSCs and glycine induced currents should be abolished in the knockout mice. However, the situation is more complex, because given retinal neurons express more than one type of synaptic GlyR (Majumdar *et al.* 2007; Weiss *et al.* 2008) and the following complications have to be considered.

(1) It is possible that a retinal neuron expresses two different types of GlyRs at the *same* postsynaptic site: immunostainings have shown coincidences of α2 and α3

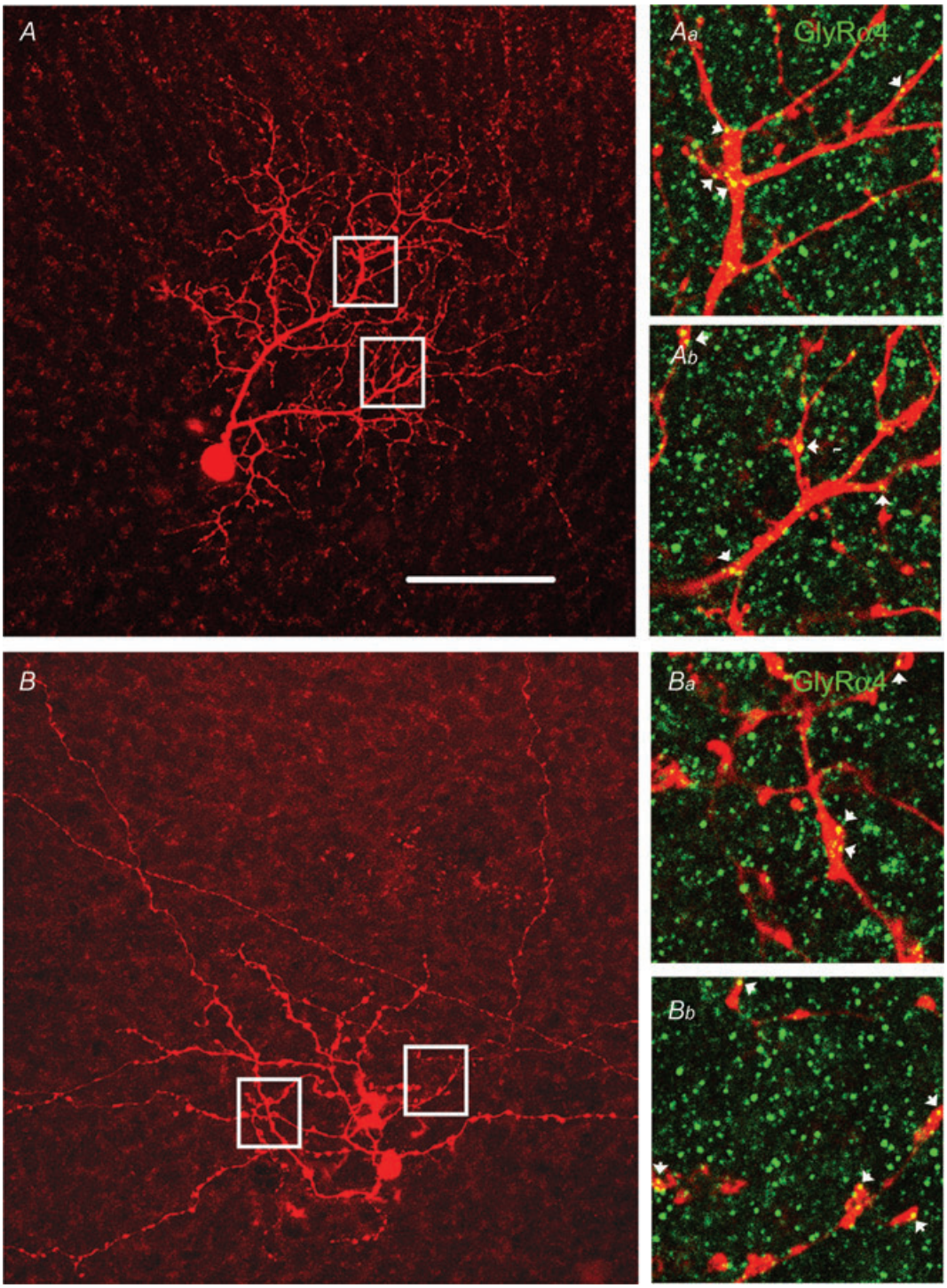

Figure 8. Colocalization of GlyR synaptic clusters with dendrites of widefield amacrine cells
A, MA-S1 (group I) cell filled with Alexa 568 and neurobiotin during the whole cell recordings. The boxed areas are shown at higher magnification in *Aa* and *Ab*. The green puncta in *Aa* and *Ab* represent GlyRα4 immunoreactive synaptic clusters. The arrowheads indicate clusters that coincide with the dendrites of the MA-S1 cell. *B*, PA-S4 (group II) cell. The boxed areas are shown at higher magnification in *Ba* and *Bb*. Other conventions as in *A*. Scale bar: 50 μm in *A* and *B*,12.4 μm in *Aa*, *Ab*, *Ba*, *Bb*.

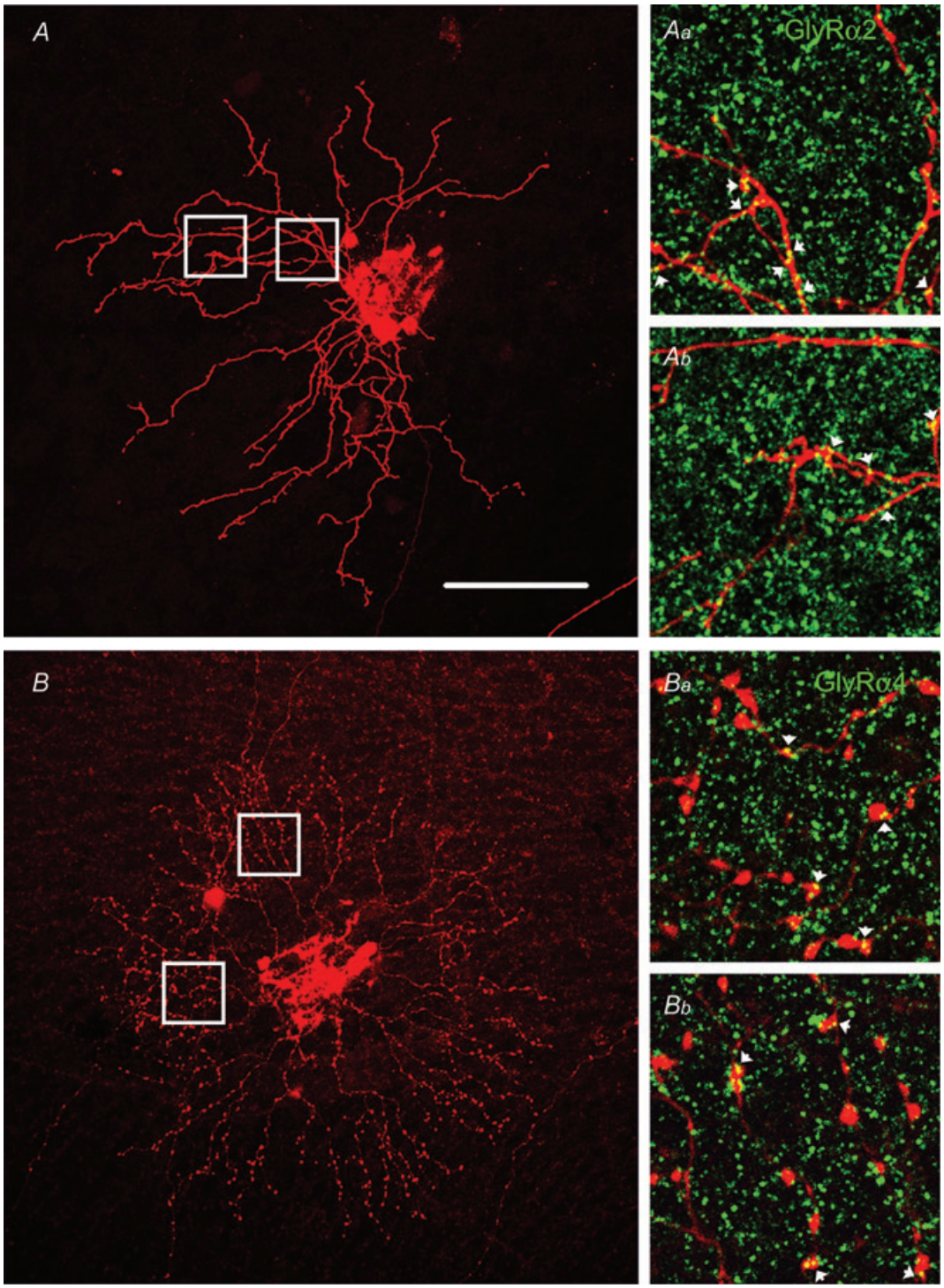

Figure 9. Colocalization of GlyR synaptic clusters with the dendrites of a MA-S5 (group I) cell (*A*) and with the dendrites of a starburst cell (*B*)
A, the MA-S5 cell was immunostained for the GlyRα2 subunit and many immunoreactive synaptic clusters coincide with the dendrites of this cell (*a* and *b*). *B*, this starburst amacrine cell was immunostained for the GlyRα4 subunit and many immunoreactive clusters coincide with dendritic varicosities of this cell (*a* and *b*). Scale bar: 50 μm in *A* and *B*, 12.4 μm in *Aa*, *Ab*, *Ba*, *Bb*.

or $\alpha 2$ and $\alpha 4$ subunits in synaptic hot spots (Haverkamp *et al.* 2003; Heinze *et al.* 2007). A vesicle released from the presynaptic terminal would activate both receptors simultaneously and the sIPSc would be the sum of the currents contributed by the two receptors.

(2) It is also possible, that the postsynaptic GlyR is composed of two different α subunits such as $\alpha 2\alpha 3\beta$ or $\alpha 2\alpha 4\beta$. Such receptors would have intrinsically different kinetics.

(3) Finally one has to consider that a given neuron expresses two types of GlyR, such as $\alpha 2\beta$ and $\alpha 4\beta$, at different input synapses, which are innervated by different presynaptic neurons. Recordings of the sIPSCs would reveal those mediated by the $\alpha 2\beta$ and those contributed by the $\alpha 4\beta$ GlyRs, resulting in a broad histogram of decay time constants. The two input neurons do not necessarily have to be spontaneously active under the recording conditions of the present study. Therefore, immunostaining of hot spots and the recordings of sIPSCs may differ.

Keeping these provisos in mind, the results of the present paper can be explained as follows.

Group II widefield amacrine cells (PA-S4, WA-S3, and WA-multi) showed small or no glycine induced currents in *Glra2*$^{-/-}$ mice and no sIPSCs could be recorded in these mutants. This suggests that the great majority of synaptic GlyRs of group II cells are $\alpha 2\beta$ receptors. However, immunostaining has shown that group II cells express also the $\alpha 4$ subunit (Fig. 7*B*) and the histogram of decay time constants in the *Glra1*$^{spd\text{-}ot}$ mouse is shifted to longer τ values (Fig. 4*F*). This would suggest group II widefield cells receive also a small additional glycinergic input, which does not show up so much under the recording conditions of the present experiment.

Group I widefield amacrine cells (MA-S5, MA-S1, MA-S1/S5, A17, PA-S5, PA-S1 and WA-S1) showed no significant reductions of glycine induced currents when wild-type and the three mutant mice were compared (Fig. 2*C*). There was also not much difference between wild-type and mutant mice in the kinetics and frequency distribution of τ values (Fig. 4). This leaves the possibility that GlyRs of group I cells are $\alpha 4\beta$ receptors, with kinetic properties similar to $\alpha 2\beta$ receptors. The immunocytochemical results (Fig. 8*A*) have shown that GlyR$\alpha 4$ immunoreactive hot spots are present on group I amacrine cell dendrites. However, GlyR$\alpha 2$ immunoreactive hot spots are also present on the processes of group I cells (Fig. 9*A*). Taken together the results suggest that GlyRs of group I cells are not dominated by a single subunit but probably involve both the $\alpha 2$ and $\alpha 4$ subunits.

Glycine-evoked currents in starburst amacrine cells were reduced by approximately 50% in *Glra2*$^{-/-}$ mice (Fig. 2*B*). This difference is statistically significant, and would suggest that the $\alpha 2$ subunit contributes to the glycine induced currents of starburst cells. A loss of slowly decaying $\alpha 2$ receptors would also explain the leftward shift in the cumulative decay τ histogram (Fig. 7*C*) observed with the $\alpha 2$ knockout mouse. In support of $\alpha 2$ expressing synapses on starburst cells, immunocytochemical evidence of $\alpha 2$ hot spots on these cells was found. However, the immunocytochemical staining has also shown that $\alpha 4$ immunoreactive hot spots are found at high density on ON-starburst cell dendrites (Fig. 9*B* and Heinze *et al.* 2007). No changes in the distribution of the decay time constants, τ, of starburst cells were observed between wild-type, *Glra1*$^{spd\text{-}ot}$ mice and *Glra3*$^{-/-}$ mice, which suggests that the $\alpha 1$ and $\alpha 3$ subunits are not involved. This leaves the $\alpha 2$ and $\alpha 4$ subunits as candidates and predicts that the histogram of the decay time constants of the *Glra2*$^{-/-}$ mouse (Fig. 5*D*) is preferentially based on GlyRs expressing the $\alpha 4$ subunit. It also suggests that synaptic $\alpha 4\beta$ GlyRs have very slow kinetics.

The decay time histograms of starburst amacrine cells showed a great variability. One reason for this could be that the data comprise fewer events from more cells, which would suggest a large cell to cell variability (see supplemental Fig. 1). However, it is also possible that starburst cells receive glycinergic synaptic input from several different presynaptic cells through synapses expressing different GlyRs such as $\alpha 2\beta$ and $\alpha 4\beta$. As mentioned above (point 3), this would result in a broad histogram of decay time constants.

Glycinergic synapses in the mouse retina

All four α subunits of the GlyR show characteristic distributions across the IPL of the mouse retina (Heinze *et al.* 2007). The $\alpha 1$ subunit is clustered in large synaptic hot spots in the OFF-sublamina, which represent synapses from AII amacrine cells onto OFF-bipolar cell axon terminals (Sassoè-Pognetto *et al.* 1994). The $\alpha 1$ immunoreactive puncta in the inner IPL are located on rod bipolar cells (Ivanova *et al.* 2006) and ganglion cell dendrites (Majumdar *et al.* 2007). Studies with recombinant GlyRs have shown that the expression of the $\alpha 1$ subunit results in channels with fast kinetics (Harvey *et al.* 2000; Legendre, 2001; Lynch, 2004; Betz & Laube, 2006). Spontaneous, GlyR-mediated synaptic currents (sIPSCs) recorded from the brainstem have shown the $\alpha 1$-containing synapses have fast decay time constants (τ ~6 ms; Singer *et al.* 1998). OFF-cone bipolar cells, rod bipolar cells and A-type ganglion cells of the mouse retina, all expressing $\alpha 1$-containing synapses have also fast decay time constants (τ bip ~5.9 ms, τ gang ~3.9 ms; Ivanova *et al.* 2006; Majumdar *et al.* 2007).

GlyR$\alpha 2$ immunoreactive synapses have been found to be distributed more evenly across the IPL (Haverkamp *et al.* 2004). Glycinergic synapses expressing the $\alpha 2$ subunit are the most frequent type of glycinergic synapses in the mouse IPL (Haverkamp *et al.* 2004). They are not expressed by bipolar cells (Ivanova *et al.* 2006), but

are confined to amacrine and ganglion cells. Since in the neonatal brainstem and spinal cord GlyRα2 is the predominant subunit (Becker *et al.* 1988; Malosio *et al.* 1991; Takahashi *et al.* 1992; Singer *et al.* 1998; Smith *et al.* 2000), it was possible to study the kinetics of GlyRα2 expressing synapses. Spontaneous IPSCs recorded from neonatal GlyR expressing the GlyRα2 subunit had slow decay time constants (τ ~14 ms; Singer *et al.* 1998). In the retina it has recently been demonstrated that narrowfield (NF) amacrine cells receive their predominant glycinergic input through GlyRα2 containing synapses and spontaneous IPSCs recorded from these synapses too had slow decay time constants (τ ~27 ms; Weiss *et al.* 2008). In the present study it was found that group II widefield amacrine cells receive their predominant glycinergic input through GlyRs containing the α2 subunit. Their mean decay time constant was 26.8 ± 9.8 ms, similar to the decay time constant of NF amacrine cells.

GlyRα3 expressing synapses have been described in the dorsal horn of the spinal cord (Harvey *et al.* 2004); however, their kinetic parameters are not yet known in detail (Heindl *et al.* 2007). GlyRα3 expressing synapses in the mouse retina are aggregated in four sublayers of the IPL. Their density is reduced along the two sublayers where the dendrites of starburst amacrine cells are found. Physiological recordings have shown that AII amacrine cells express glycinergic synapses containing the GlyRα3 subunit (Weiss *et al.* 2008). Spontaneous IPSCs recorded from AII cells had decay time constants (τ ~11 ms) which were slower than those of GlyRα1 expressing synapses and faster than those of GlyRα2 expressing synapses.

GlyRα4 expressing synapses have been described until now only in the mammalian retina (Heinze *et al.* 2007). They are sparsely distributed across the IPL with a significantly higher density within the sublamina where the processes of ON-starburst amacrine cells ramify. The kinetics of sIPSCs of GlyRα4 containing synapses can only be estimated from circumstantial evidence. As mentioned above, sIPSCs of NF amacrine cells receive their predominant glycinergic input through GlyRα2 expressing synapses. However, in the *Glra2*$^{-/-}$ mouse NF amacrine cells still received a small number of slow glycinergic sIPSCs, which most likely are based on GlyRα4 containing synapses. The decay time constants of these slow sIPSCs (τ ~70 ms) were even slower than those of GlyRα2 expressing synapses (Weiss *et al.* 2008). In the present study it was found that glycinergic sIPSCs recorded in ON-starburst amacrine cells of GlyRα2 knockout mice are dominated by GlyRs expressing the α4 subunit. The mean decay time constant τ was 53.4 ± 93 ms. In conclusion, synaptic GlyRs of the retina expressing the α1 subunit have fast kinetics, those expressing the α3 subunit have intermediate kinetics, and GlyRs containing the α2 and α4 subunits have slow kinetics.

The function of glycinergic inhibition amongst amacrine cells has recently been studied by Hsueh *et al.* (2008) in the rabbit retina. They showed that the majority of ON amacrine cells receive glycinergic OFF inhibition. About half of the OFF amacrine cells received glycinergic ON inhibition. The most common interaction between amacrine cells is, therefore, 'crossover inhibition', where OFF inhibits ON and ON inhibits OFF. The temporal fine tuning of these interactions might be the result of the different kinetics of GlyRs expressing specific α subunits.

References

Badea TC & Nathans J (2004). Quantitative analysis of neuronal morphologies in the mouse retina visualized by using a genetically directed reporter. *J Comp Neurol* **480**, 331–351.

Barry PH (1994). JPCalc, a software package for calculating liquid junction potential corrections in patch-clamp, intracellular, epithelial and bilayer measurements and for correcting junction potential measurements. *J Neurosci Methods* **51**, 107–116.

Becker CM, Hoch W & Betz H (1988). Glycine receptor heterogeneity in rat spinal cord during postnatal development. *EMBO J* **7**, 3717–3726.

Betz H & Laube B (2006). Glycine receptors: recent insights into their structural organization and functional diversity. *J Neurochem* **97**, 1600–1610.

Brandon C (1985). Retinal GABA neurons – localization in vertebrate species using an antiserum to rabbit brain glutamate-decarboxylase. *Brain Res* **344**, 286–295.

Buckwalter MS, Cook SA, Davisson MT, White WF & Camper SA (1994). A frameshift mutation in the mouse α1 glycine receptor gene (Glra1) results in progressive neurological symptoms and juvenile death. *Hum Mol Genet* **3**, 2025–2030.

Cui JJ, Ma YP, Lipton SA & Pan ZH (2003). Glycine receptors and glycinergic synaptic input at the axon terminals of mammalian retinal rod bipolar cells. *J Physiol* **553**, 895–909.

Dodt HU & Zieglgänsberger W (1990). Visualizing unstained neurons in living brain slices by infrared DIC-videomicroscopy. *Brain Res* **537**, 333–336.

Eggers ED & Lukasiewicz PD (2006). Receptor and transmitter release properties set the time course of retinal inhibition. *J Neurosci* **26**, 9413–9425.

Fischer F, Kneussel M, Tintrup H, Haverkamp S, Rauen T, Betz H & Wässle H (2000). Reduced synaptic clustering of GABA and glycine receptors in the retina of the gephyrin null mutant mouse. *J Comp Neurol* **427**, 634–648.

Frech MJ, Pérez-León J, Wässle H & Backus KH (2001). Characterization of the spontaneous synaptic activity of amacrine cells in the mouse retina. *J Neurophysiol* **86**, 1632–1643.

Gill SB, Veruki ML & Hartveit E (2006). Functional properties of spontaneous IPSCs and glycine receptors in rod amacrine (AII) cells in the rat retina. *J Physiol* **575**, 739–759.

Grudzinska J, Schemm R, Haeger S, Nicke A, Schmalzing G, Betz H & Laube B (2005). The β subunit determines the ligand binding properties of synaptic glycine receptors. *Neuron* **45**, 727–739.

Harvey RJ & Betz H (2000). Structure, diversity, pharmacology, and pathology of glycine receptor chloride channels. In *Handb Exp Pharmacol* **147**, 479–497.

Harvey RJ, Depner UB, Wässle H, Ahmadi S, Heindl C, Reinold H, Smart TG, Harvey K, Schütz B, Abo-Salem OM, Zimmer A, Poisbeau P, Welzl H, Wolfer DP, Betz H, Zeilhofer HU & Müller U (2004). GlyR α3: an essential target for spinal PGE2-mediated inflammatory pain sensitization. *Science* **304**, 884–887.

Haverkamp S, Müller U, Harvey K, Harvey RJ, Betz H & Wässle H (2003). Diversity of glycine receptors in the mouse retina: localization of the α3 subunit. *J Comp Neurol* **465**, 524–539.

Haverkamp S, Müller U, Zeilhofer HU, Harvey RJ & Wässle H (2004). Diversity of glycine receptors in the mouse retina: localization of the α2 subunit. *J Comp Neurol* **477**, 399–411.

Harvey RJ, Schmieden V, Von Holst A, Laube B, Rohrer H & Betz H (2000). Glycine receptors containing the α4 subunit in the embryonic sympathetic nervous system, spinal cord and male genital ridge. *Eur J Neurosci* **12**, 994–1001.

Heindl C, Brune K & Renner B (2007). Kinetics and functional characterization of the glycine receptor α2 and α3 subunit. *Neurosci Lett* **429**, 59–63.

Heinze L, Harvey RJ, Haverkamp S & Wässle H (2007). Diversity of glycine receptors in the mouse retina: localization of the α4 subunit. *J Comp Neurol* **500**, 693–707.

Hsueh, H-A, Molnar A & Werblin FS (2008). Amacrine-to-amacrine cell inhibition in the rabbit retina. *J Neurophysiol* **100**, 2077–2088.

Hughes A & Wieniawa-Narkiewicz E (1980). A newly identified population of presumptive microneurones in the cat retinal ganglion cell layer. *Nature* **284**, 468–470.

Ivanova E, Müller U & Wässle H (2006). Characterization of the glycinergic input to bipolar cells of the mouse retina. *Eur J Neurosci* **23**, 350–364.

Kling C, Koch M, Saul B & Becker CM (1997). The frameshift mutation oscillator (Glra1 (spd-ot)) produces a complete loss of glycine receptor α1-polypeptide in mouse central nervous system. *J Neurosci* **78**, 411–417.

Kneussel M, Hermann A, Kirsch J & Betz H (1999). Hydrophobic interactions mediate binding of the glycine receptor β-subunit to gephyrin. *J Neurochem* **72**, 1323–1326.

Kneussel M & Betz H (2000). Receptors, gephyrin and gephyrin-associated proteins: novel insights into the assembly of inhibitory postsynaptic membrane specializations. *J Physiol* **525**, 1–9.

Legendre P (2001). The glycinergic inhibitory synapse. *Cell Mol Life Sci* **58**, 760–793.

Lin B & Masland RH (2006). Populations of wide-field amacrine cells in the mouse retina. *J Comp Neurol* **499**, 797–809.

Lynch JW (2004). Molecular structure and function of the glycine receptor chloride channel. *Physiol Rev* **84**, 1051–1095.

MacNeil MA & Masland (1998). Extreme diversity among amacrine cells: implications for function. *Neuron* **20**, 971–982.

Majumdar S, Heinze L, Haverkamp S, Ivanova E & Wässle H (2007). Glycine receptors of A-type ganglion cells of the mouse retina. *Vis Neurosci* **24**, 471–487.

Malosio ML, Marquèze-Pouey B, Kuhse J & Betz H (1991). Widespread expression of glycine receptor subunit mRNAs in the adult and developing rat brain. *EMBO J* **10**, 2401–2409.

Masland RH (2001). The fundamental plan of the retina. *Nat Neurosci* **4**, 877–886.

Menger N, Pow DV & Wässle H (1998). Glycinergic amacrine cells of the rat retina. *J Comp Neurol* **401**, 34–46.

Pérez De Sevilla Müller L, Shelley J & Weiler R (2007). Displaced amacrine cells of the mouse retina. *J Comp Neurol* **505**, 177–189.

Pérez-León J, Frech MJ, Schröder JE, Fischer F, Kneussel M, Wässle H & Backus KH (2003). Spontaneous synaptic activity in an organotypic culture of the mouse retina. *Invest Ophthalmol Visual Sci* **44**, 1376–1387.

Perry VH (1981). Evidence for an amacrine cell system in the ganglion cell layer of the rat retina. *Neuroscience* **6**, 931–944.

Pourcho RG & Goebel DJ (1985). A combined Golgi and autoradiographic study of (^{3}H)glycine-accumulating amacrine cells in the cat retina. *J Comp Neurol* **233**, 473–480.

Protti DA, Gerschenfeld HM & Llano I (1997). GABAergic and glycinergic IPSCs in ganglion cells of rat retinal slices. *J Neurosci* **17**, 6075–6085.

Sandell JH & Masland RH (1986). A system of indoleamine-accumulating neurons in the rabbit retina. *J Neurosci* **6**, 3331–3347.

Sassoè-Pognetto M, Wässle H & Grünert U (1994). Glycinergic synapses in the rod pathway of the rat retina: cone bipolar cells express the α1 subunit of the glycine receptor. *J Neurosci* **14**, 5131–5146.

Singer JH, Talley EM, Bayliss DA & Berger AJ (1998). Development of glycinergic synaptic transmission to rat brain stem motoneurons. *J Neurophysiol* **80**, 2608–2620.

Smith AJ, Owens S & Forsythe ID (2000). Characterisation of inhibitory and excitatory postsynaptic currents of the rat medial superior olive. *J Physiol* **529**, 681–698.

Takahashi T, Momiyama A, Hirai K, Hishinuma F & Akagi H (1992). Functional correlation of fetal and adult forms of glycine receptors with developmental changes in inhibitory synaptic receptor channels. *Neuron* **9**, 1155–1161.

Tian N, Hwang TN & Copenhagen DR (1998). Analysis of excitatory and inhibitory spontaneous synaptic activity in mouse retinal ganglion cells. *J Neurophysiol* **80**, 1327–1340.

Veruki ML, Gill SB & Hartveit E (2007). Spontaneous IPSCs and glycine receptors with slow kinetics in wide-field amacrine cells in the mature rat retina. *J Physiol* **581**, 203–219.

Wässle H (2004). Parallel processing in the mammalian retina. *Nat Rev Neurosci* **5**, 747–757.

Wässle H, Chun MH & Müller F (1987*b*). Amacrine cells in the ganglion cell layer of the cat retina. *J Comp Neurol* **265**, 391–408.

Wässle H, Voigt T & Patel B (1987*a*). Morphological and immunocytochemical identification of indoleamine-accumulating neurons in the cat retina. *J Neurosci* **7**, 1574–1585.

Weiss J, O'Sullivan GA, Heinze L, Chen HX, Betz H & Wässle H (2008). Glycinergic input of small-field amacrine cells in the retinas of wildtype and glycine receptor deficient mice. *Mol Cell Neurosci* **37**, 40–55.

Young-Pearse TL, Ivic L, Kriegstein AR & Cepko CL (2006). Characterization of mice with targeted deletion of glycine receptor α2. *Mol Cell Biol* **26**, 5728–5734.

Author contributions

All three authors have contributed to the conception and design, or analysis and interpretation of the data, drafting the article or revising it critically for important intellectual content, and final approval to the version to be published. The experiments have largely been performed by Sriparna Majumdar.

Acknowledgements

We are grateful to Dr Ulrike Müller for providing the Glra3$^{-/-}$ mouse, to Dr Heinrich Betz for providing the Glra2$^{-/-}$ mouse and to Dr R. J. Harvey for the gift of antibodies against the GlyRα4 subunit. We thank Brigitte Sinke for excellent technical assistance and Irmgard Odenthal for typing the manuscript.